Arch. Metall. Mater. **68** (2023), 4, 1383-1390

DOI: https://doi.org/10.24425/amm.2023.146204

JIA LIU[1,2*], JITUO LIU[3], XIANHUI WANG[3]

STUDY ON PHASE TRANSFORMATION DYNAMICS, MICROSTRUCTURE, AND PROPERTIES OF THE Cu-2.7Ti-2.5Ni-0.8V ALLOY

The phase transformation dynamic and electrical conductivity equations of the aged Cu-2.7Ti-2.5Ni-0.8V alloy were established in this work. The microstructure evolution and precipitated phases were characterized by scanning electron microscopy (SEM) and transmission electron microscopy (TEM). The mechanical properties were tested using a hardness testing machine and universal test machine, and the electrical conductivity was measured by the eddy conductivity gauge. The results show that NiTi intermetallic compounds are formed during the solidification, and these phases such as Ni_3Ti and NiV_3 are precipitated after aging treatment. The fracture morphology displays that a large number of shallow and equiaxed dimples occur on the tensile fracture, indicating a typical ductile fracture. After aging treatment at 450°C for 240 min, the hardness, tensile strength, elongation and electrical conductivity of the Cu-2.7Ti-2.5Ni-0.8V alloy are 184 HV, 459 MPa, 6.3% and 28.72% IACS, respectively.

Keywords: Cu alloy; Precipitation; Microstructure; Properties

1. Introduction

Due to the good electrical thermal and electrical conductivity, excellent mechanical properties, anti-fatigue and anti-corrosion performance, copper alloys are used widely in the various fields such as integrated circuit lead frames, conductive devices, instrumentation, computer and communication technology, and precision machinery manufacturing [1-4]. With the development of electrical devices and apparatus towards lightweight, miniaturization, multi-functionalization and harmless eco-environment, the increasingly stringent requirements are put forward for copper alloys, such as high electrical conductivity, excellent strength, low manufacturing cost, and friendly to the environment [5-8]. Currently, Cu-Be alloy has a good comprehensive property, but it has prohibitory cost and toxic substances such as beryllium oxide formed during the production process hinder its applications. Additionally, its manufacturing process is complicated, and Cu-Be alloy displays poor high-temperature stability [9-11]. Subsequently, it is necessary to develop a new environmentally-friendly copper alloy with excellent mechanical properties, electrical conductivity, and high-temperature properties.

Cu-Ti alloy exhibits a good combination of mechanical properties, corrosion resistance, anti-abrasion resistance, workability, weldability and excellent anti-stress relaxation property at elevated temperatures, and the production process does not possess hazards to humanity health and environment, it is regarded as an ideal substitute to Cu-Be alloy [12-15]. However, the large solubility of Ti atoms in the Cu matrix causes electron scattering, thus resulting in the decrease on the electrical conductivity. It is difficult to simultaneously achieve high strength and good electrical conductivity for Cu-Ti alloy. Hence, it poses a challenge for material researchers to improve its electrical conductivity while its excellent mechanical properties can be still maintained [16]. Thus far, a number of investigations shows that it is an effective measure to incorporate trace alloying elements in the Cu-Ti alloy, such as Fe [17], Cr [18], Co [14, 19], Cd [20], Sn [21], Al [22], P [23], which can reduce the Ti solid solution in the Cu matrix and form the intermetallic compounds, thereby reducing electron scattering and improving the electrical conductivity.

In our previous work, we studied the effect of Ni element on the microstructure and properties of Cu-3Ti alloy, and found that the incorporation of Ni is beneficial for the improvement of electrical conductivity, but it is hard to achieve the good tradeoff for the electrical conductivity and mechanical properties [24,25]. Due to the greater affinity between V and Ni, V can combine with Ni to form intermetallic compound [26-28]. This was verified by

[1] XI'AN POLYTECHNIC UNIVERSITY, SCHOOL OF MATERIALS SCIENCE AND ENGINEERING, XI'AN 710048, P.R. CHINA
[2] XI'AN UNIVERSITY OF TECHNOLOGY, SCHOOL OF MECHANICAL AND PRECISION INSTRUMENT ENGINEERING, XI'AN 710048, P. R. CHINA
[3] XI'AN UNIVERSITY OF TECHNOLOGY, SCHOOL OF MATERIALS SCIENCE AND ENGINEERING, XI'AN 710048, P. R. CHINA

* Corresponding author: liujia09200920@163.com

a few literatures [29-32]. More importantly, it is also reported that V addition can enhance the mechanical properties and has minor effect on the electric conductivity of Cu-3.2Ti-0.2Fe alloys [33]. To further enhance the electrical conductivity and sustain its mechanical properties of Cu-Ti-Ni alloy, V addition was introduced into the Cu-Ti-Ni alloy in this work. The phase transformation dynamics and electrical conductivity equations of the aged Cu-2.7Ti-2.5Ni-0.8V alloy at different temperatures were established, and the effect of the aging process on the microstructure and properties of Cu-2.7Ti-2.5Ni-0.8V alloy was studied. The research can provide the reference for the design and manufacture of conductive copper alloys with excellent comprehensive properties.

2. Experimental procedures

An as-cast ingot of Cu-2.7wt%Ti-2.5wt%Ni-0.8wt%V alloy was fabricated by a vacuum intermediate frequency induction furnace from the raw materials of 99.9wt% pure copper, 99.9wt% sponge titanium, 99.9wt% nickel, and 99.9wt% vanadium. The ingots were cut into blocks by

wire cutting machine. Then, the blocks were homogenized at 900°C for 6 h and solubilized at 850°C for 4 h in an atmosphere tube furnace, followed by quenching into water. The specimens were aged at 350, 400, 450 and 500°C for 15, 30, 45, 60, 90, 120, 150, 180, 240, 300, 360, 420, 480, 540, 600, 660 min. Homogenization, solution, and aging treatments were performed in TL1200 tube furnace under the protection of argon gas.

The specimens for microstructural examination were mechanically polished and subsequently etched in the solution of 5 g $FeCl_3$, 15 mL HCl and 100 mL distilled water. The morphology and phases were characterized by JSM-6700F scanning electron microscope (SEM) equipped with energy disperse spectrometer (EDS) and JEM-2100 transmission electron microscope (TEM). The specimens used for TEM observations were cut from the aged samples, and then mechanically polished to obtain the slices with the thickness of 40~60 μm. Discs of 3 mm diameter were punched from these slices and thinned in an M691 ion milling machine at 4.5 kV. Electrical conductivity, hardness, and tensile strength were measured by MH-3 version hardness meter, D60K digital metal conductivity measuring instrument, and UTM5504 universal testing machine.

3. Results and discussion

3.1. Dynamics of phase transformation

During aging treatment, the electrical conductivity of the Cu-2.7Ti-2.5Ni-0.8V alloy increase with increase of the aging time. At the beginning of aging, the electrical conductivity and the phase volume fraction (f) are denoted as σ_0 and 0, respectively. In addition, solute atoms have large supersaturated concentrations in the Cu matrix at the beginning of aging, which promote the precipitation, and the precipitation power of solute atoms is relatively large. Therefore, the electrical conductivity increases sharply at the initial stage. After holding for a long aging time, the precipitation is completed, the electrical conductivity reaches σ_{max} and the volume fraction of the precipitated phase is $f = 1$. The relationship between the volume fraction of the precipitation phase and the alloy's electrical conductivity can be expressed as follows [34-36].

$$\sigma = \sigma_0 + Af \tag{1}$$

$$A = \sigma_{max} - \sigma_0 \tag{2}$$

The volume fraction of the precipitated phase can be calculated using Eqs. (1)-(2), and the value of σ can be measured after aging for different times.

The relationship between the aging time t and the volume fraction of the precipitated phase f is as follows:

$$f = 1 - \exp(-bt^n) \tag{3}$$

where n and b are constants, the parameter n depends on the nucleation location and the type of phase transformation, while b depends on the composition of the supersaturated solid solution and the phase transformation temperature.

From Eqs. (1)-(3), the electrical conductivity can be written:

$$\sigma = \sigma_0 + (\sigma_{max} - \sigma_0)[1 - \exp(-bt^n)] \tag{4}$$

Eq. (3) can transform into Eq. (5):

$$1 - f = \exp(-bt^n) \tag{5}$$

By taking the log of Eq. (5):

$$\lg[\ln(1-f)^{-1}] = \lg b + n \lg t \tag{6}$$

The relationship between $\lg[\ln(1-f)^{-1}]$ and $\lg t$, Fig. 1, is approximately a straight line, which we can use to determine the $\lg b$ as the intercept and n as the slope of the line.

The Avrami method applied to the electrical conductivity and the phase transformation dynamics for the Cu-2.7Ti-2.5Ni-0.8V alloy aged at 350, 400, 450, and 500°C are expressed in TABLE 1.

According to Fig. 1 and TABLE 1, the dynamics curve of the precipitation phase transformation of the Cu-2.7Ti-2.5Ni-0.8V alloy at different temperatures can be obtained. Fig. 2 shows the phase transformation rate increases as a function of the aging time. However, the phase transformation rate gradually decreases until the equilibrium state is reached. As a result, the solid solution atoms in the Cu matrix can be precipitated in the form of the secondary phase during aging, resulting in the improvement on the electrical conductivity and the precipitated phase volume fraction with aging time. Nevertheless, as the aging time increases, the decreased solid solution can increase the electrical conductivity, and the volume fraction of the precipitate phase progressively approaches a constant value.

Fig. 3 shows the comparison between the calculated electrical conductivity and the measures values. Apparently,

TABLE 1

The equations of phase transformation dynamics and electrical conductivity for the Cu-2.7Ti-2.5Ni-0.8V alloy aged at different temperatures

	The equations of phase transformation dynamics	The equations of electrical conductivity
350°C	$f = 1 - \exp(-0.000541t^{1.50209})$	$\sigma = 15.84 + 11.11[1 - \exp(-0.000541t^{1.50209})]$
400°C	$f = 1 - \exp(-0.003608t^{1.17195})$	$\sigma = 15.84 + 11.97[1 - \exp(-0.0003608t^{1.17195})]$
450°C	$f = 1 - \exp(-0.008429t^{1.03012})$	$\sigma = 15.84 + 12.88[1 - \exp(-0.008429t^{1.03012})]$
500°C	$f = 1 - \exp(-0.008342t^{1.04253})$	$\sigma = 15.84 + 14.39[1 - \exp(-0.008342t^{1.04253})]$

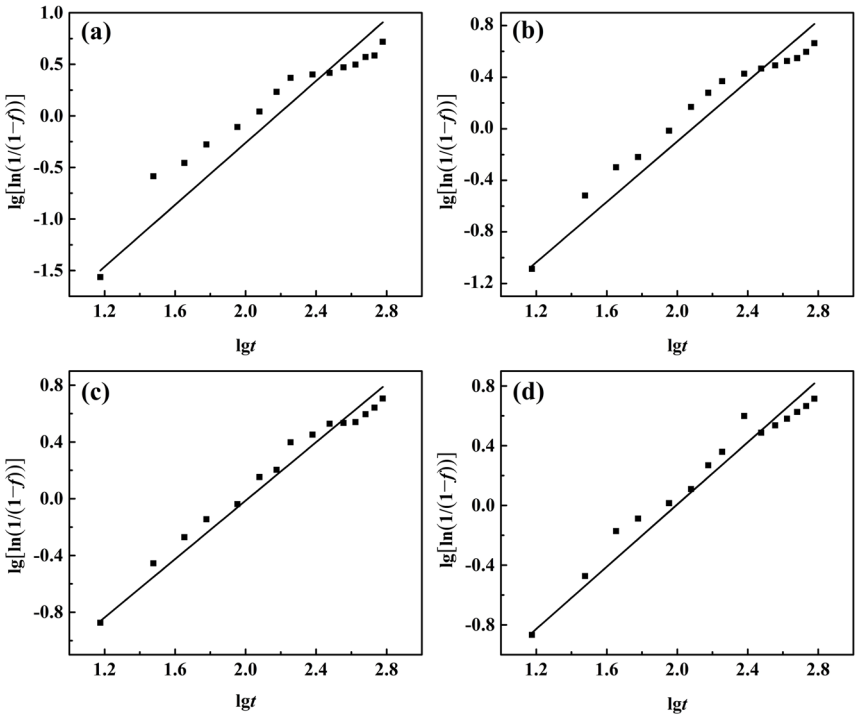

Fig. 1. The relation of $\lg[\ln(1-f)^{-1}]$ and $\lg t$ for the Cu-2.7Ti-2.5Ni-0.8V alloy after aging at different temperatures: (a) 350°C; (b) 400°C; (c) 450°C; (d) 500°C

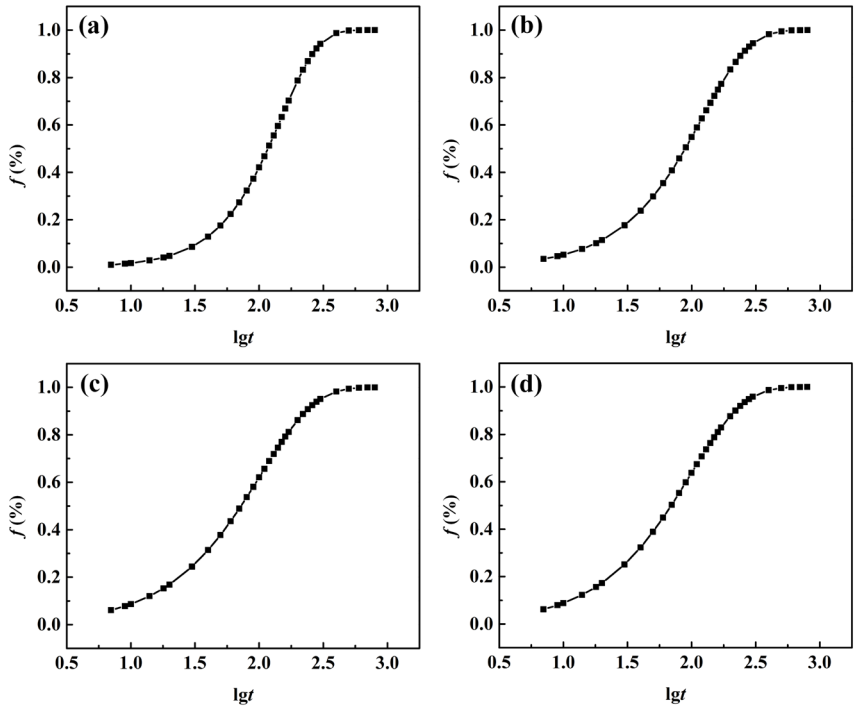

Fig. 2. Phase transformation dynamics as function of aging temperature: (a) 350°C; (b) 400°C; (c) 450°C; (d) 500°C

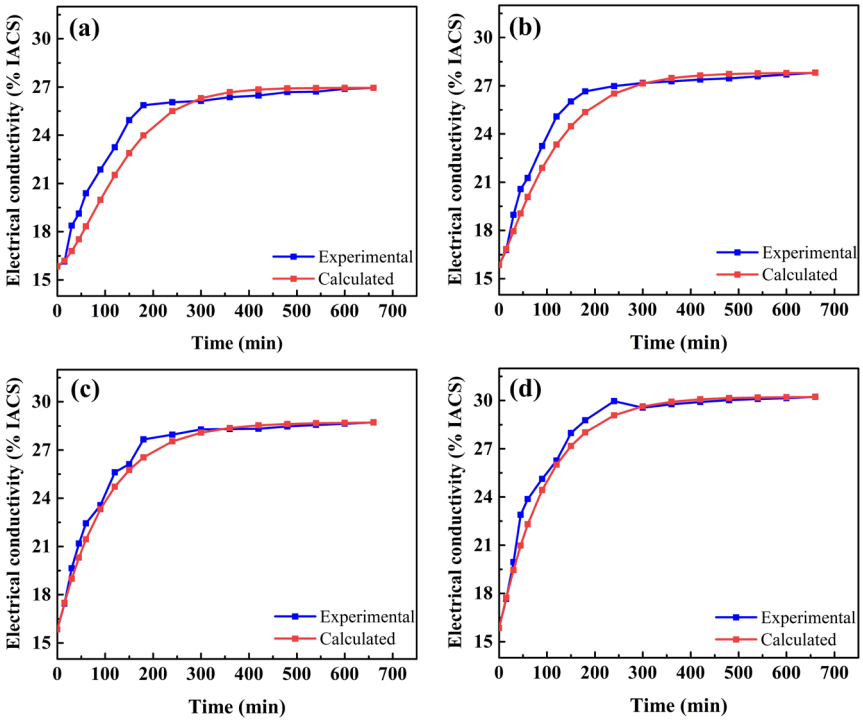

Fig. 3. Comparison of predicted value and measured data for the electrical conductivity of Cu-2.7Ti-2.5Ni-0.8V alloy after aging at different temperatures: (a) 350°C; (b) 400°C; (c) 450°C; (d) 500°C

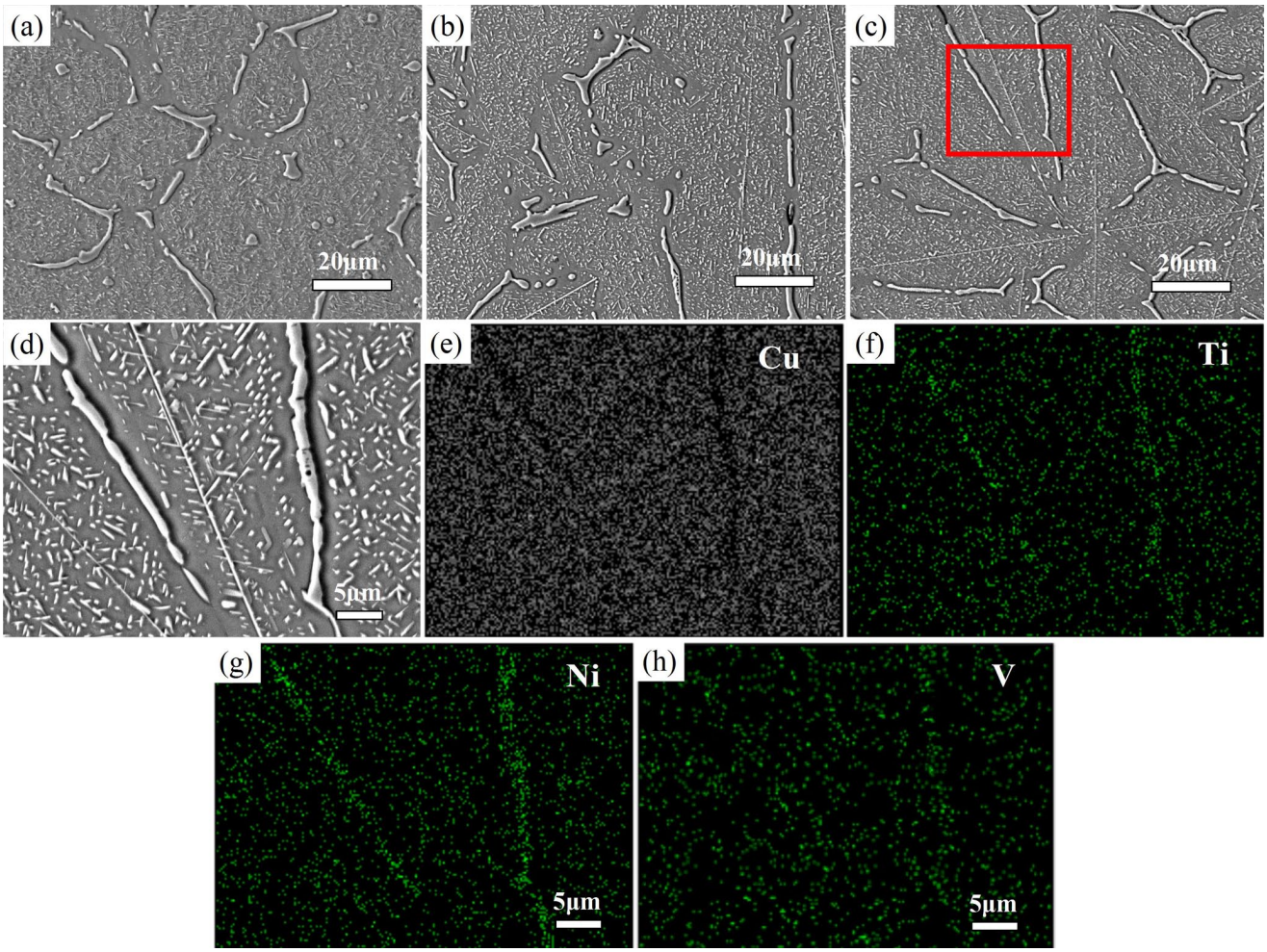

Fig. 4. SEM micrographs and the elemental mapping images of Cu-2.7Ti-2.5Ni-0.8V alloy after aging at 450°C for different time: (a) 30 min; (b) 120 min; (c) 240 min; (d) The micrograph of (c) at high magnification; (e) Cu element; (f) Ti element; (g) Ni element; (h) V element

the measured values are in good agreement with the calculated results, indicating that the equation can accurately predict the electrical conductivity at different aging temperatures and time.

3.2. Microstructural characterization

Fig. 4 shows the SEM micrographs and the EDS results of Cu-2.7Ti-2.5Ni-0.8V alloy after aging at 450°C for 30, 120 and 240 min. It is visible that fine rod-like phases and irregular spherical phases are precipitated from the copper alloy matrix (Fig. 4(a)). With increase of the aging time, the precipitated phases increase gradually (Fig. 4(b)). With further increasing aging time, the precipitation phase with elongated and needle-like morphology generates in the Cu matrix, see Fig. 4(c) and Fig. 4(d). In addition, some primary phases form during solidification. To determine these primary phases, EDS analysis was performed, and the elemental mapping images are presented in Figs. 4(d)(h). It can preliminarily demonstrate that the primary phases are composed of Ni and Ti (Figs. 4(f), (g)), and V are uniformly distributed in the Cu matrix (Fig. 4(h)).

In order to determine the phase constituents, TEM analysis was performed on the sample aged at 450°C for 240 min, and the TEM images were shown in Fig. 5. Clearly, an irregular particle phase with a size of about 1μm can be observed from Fig. 5(a), and its selected area electron diffraction (SAED) pattern is displayed in Fig. 5(b). As determined from Fig. 5(b), the precipitate is NiTi phase having a monoclinic structure with lattice parameters: a = 0.2885 nm, b = 0.4622 nm, c = 0.412 nm, α = 90°, β = 96.8°, γ = 90°. Therefore, NiTi intermetallic compounds are formed during the solidification of Cu-2.7Ti-2.5Ni-0.8V alloy. It is evident from Fig. 5(c) and Fig. 5(d) that there is a lath-like precipitated phase in the Cu matrix. From Fig. 5(d), it can verify that the lath-like precipitated phase is the Ni_3Ti phase, which has a hexagonal structure with the lattice parameters: a = 0.5092 nm, b = 0.5092 nm, c = 0.8297 nm, α = 90°, β = 90°, γ = 120°. In addition, the needle-like precipitated phase can be observed from Fig. 5(e), and its SAED pattern is presented in Fig. 5(f). According to the indexed results of the SAED pattern, the needle-like precipitated phase is the NiV_3 phase, which has a cubic structure with the lattice parameters: $a = b = c$ = 0.471 nm, $\alpha = \beta = \gamma$ = 90°. Therefore, Ni_3Ti and NiV_3 phases are precipitated after aging treatment. The precipitated phases for the contacts between each other via their edges, which prevents the further forward extensions of the edges. Therefore, a plausible growth mechanism for the precipitated phase is thickening of the stripe phase.

3.3. Mechanical and electrical properties

The variation of hardness and electrical conductivity of Cu-2.7Ti-2.5Ni-0.8V alloy with aging time is presented in Figs. 6(a)-6(b). From Fig. 6(a), the hardness increases and then decreases with increase of the aging time, and the peak hardness of 184 HV can be obtained after aging treatment at 450°C for

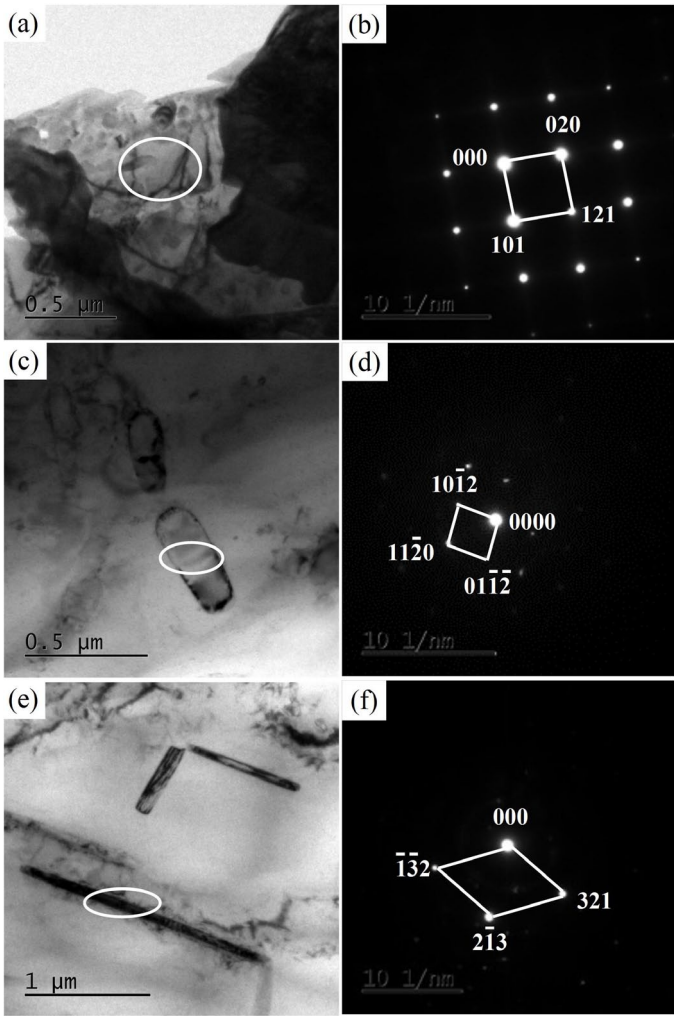

Fig. 5. TEM images (a, c, e) and corresponding SAED patterns (b, d, f) of solubilized Cu-2.7Ti-2.5Ni-0.8V alloy aging at 450°C for 240 min

240 min. This is classical precipitation hardening and the value of hardness depends on precipitates dispersion degree i.e. on size of the precipitates and distances between them. At first when the number of precipitated phases increases the hardness increases. However, the prolonged aging time causes precipitate coarsening, which progressively reduces the strengthening effect, and, thus, hardness decreases with aging time.

As seen from Fig. 6(b), the electrical conductivity of Cu-2.7Ti-2.5Ni-0.8V alloy increases rapidly and then slowly increases with increase of the aging time. This is because the large distortion energy caused by the supersaturated Ti, Ni, and V solute atoms in the Cu matrix at the initial aging stage can promote the precipitation from the Cu matrix. Since the electrical conductivity is more sensitive to solute concentration in the Cu matrix, the precipitation of Ti, Ni, and V solute atoms reduces the electron scattering and the electrical conductivity increases sharply at the initial aging stage [37]. Nevertheless, the precipitation power decreases with decrease of solute concentration in the Cu matrix, the precipitation rate of the second precipitation phase slows down gradually, and the electrical conductivity increases slowly. As a result, the electrical conductivity of the Cu-2.7Ti-2.5Ni-0.8V alloy after aging at 450°C for 240 min is 28.72% IACS.

Fig. 7 shows the variation of the tensile strength and

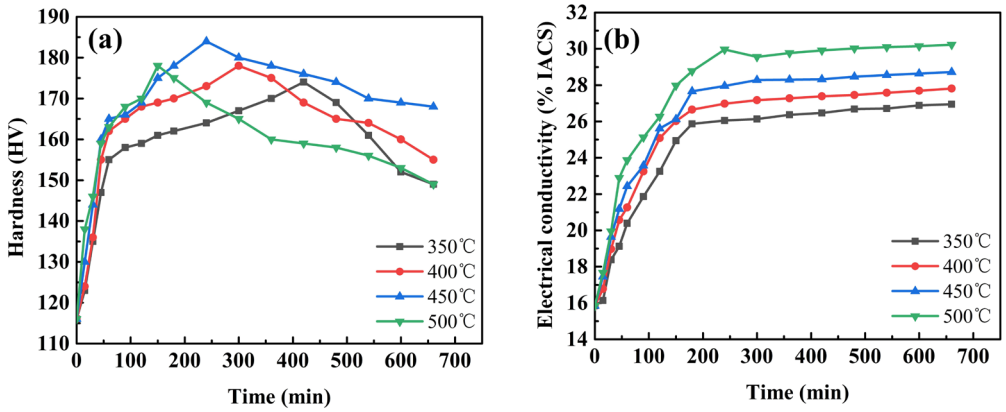

Fig. 6. Variation of the hardness and electrical conductivity of Cu-2.7Ti-2.5Ni-0.8V alloy with aging time (a) hardness; (b) electrical conductivity

elongation of Cu-2.7Ti-2.5Ni-0.8V alloy with aging time. The tensile strength increases and then decreases as a function of the aging time. However, the elongation decreases and then increases with aging time. After aging at 450°C for 240 min, the tensile strength and elongation of Cu-2.7Ti-2.5Ni-0.8V alloy are 459 MPa and 6.3%, respectively. The tensile fracture morphology of Cu-2.7Ti-2.5Ni-0.8V alloy after aging treatment at 450°C for 240 min is represented. From Fig. 8, a large amount of shallow and equiaxed dimples are observed on the fracture, revealing that the fracture mechanism of the studied alloy is ductile fracture [38].

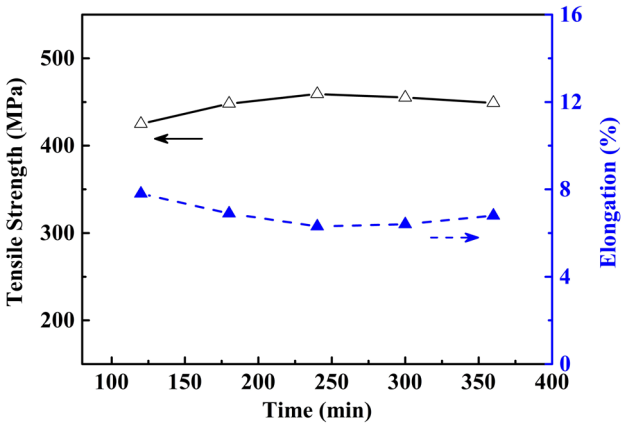

Fig. 7. Variation of the tensile strength and elongation of Cu-2.7Ti-2.5Ni-0.8V alloy with aging time

In the present work, the hardness, tensile strength and electrical conductivity of Cu-2.7Ti-2.5Ni-0.8V alloy after aging at 450°C for 240 min are 184 HV, 459 MPa and 28.72% IACS, respectively. We have conducted a number of investigations on Cu-Ti alloy. For the Cu-3Ti-1Ni alloy, the hardness and electrical conductivity are 205HV and 18.2% IACS, respectively [25]. Cu-3Ti-2Sn alloy has an electrical conductivity of 39.8% IACS and a hardness of 134.5 HV [21]. The hardness, tensile strength and electrical conductivity of Cu-3Ti-2Mg alloy are 357.6 HV, 401 MPa and 18.5%IACS [39]. Konno et al. [22] studied the effect of 4 at.% Al addition on the hardness and electrical conductivity of the Cu-3 at.% Ti alloy, and the results indicated that this ternary alloy has a peak hardness value of 180 HV, while the electrical conductivity is quite low, which is 6%IACS. Markandeya et al. [40, 41] reported that the Cu-3Ti-1Cr alloy has the tensile strength of 890 MPa and hardness of 300 HV, and Cu-3Ti-1Cd alloy has the tensile strength of 916 MPa, but no data of electrical conductivity is reported in their work. Though Cu-6Ti-0.3Fe alloy reported by Rouxel [17] can achieve higher tensile strength (975 MPa), no electrical conductivity is mentioned as well.

This study shows that V micro-addition, when combined with the appropriate amounts of Ti (2.7wt.%) and Ni (2.5wt.%), endows the good combination of electrical conductivity and mechanical properties of Cu-based alloys, providing an excellent alternative to Cu-Be in the electronic industry for bushings, bearings, springs, electronic connectors.

4. Conclusions

1) Based on the Avrami method, the phase transformation dynamics and electrical conductivity equations of the Cu-2.7Ti-2.5Ni-0.8V alloy are established at different aging temperatures and time.
2) NiTi intermetallic compounds are formed during the solidification of Cu-2.7Ti-2.5Ni-0.8V alloy, and Ni_3Ti and NiV_3 phases are precipitated after aging treatment.
3) After aging at 450°C for 240 min, the hardness, tensile strength, elongation and electrical conductivity of the Cu-2.7Ti-2.5Ni-0.8V alloy are 184 HV, 459 MPa, 6.3% and 28.72%IACS, respectively.
4) A large amount of shallow and equiaxed dimples are formed on the fracture, which reveals that the fracture mechanism of the studied alloy is ductile fracture.

Acknowledgment

This research was supported by the National Natural Science Foundation of China (No. 51971173), Science and Technology Guidance Program Project of China National Textile and Apparel Council (No. 2021039).

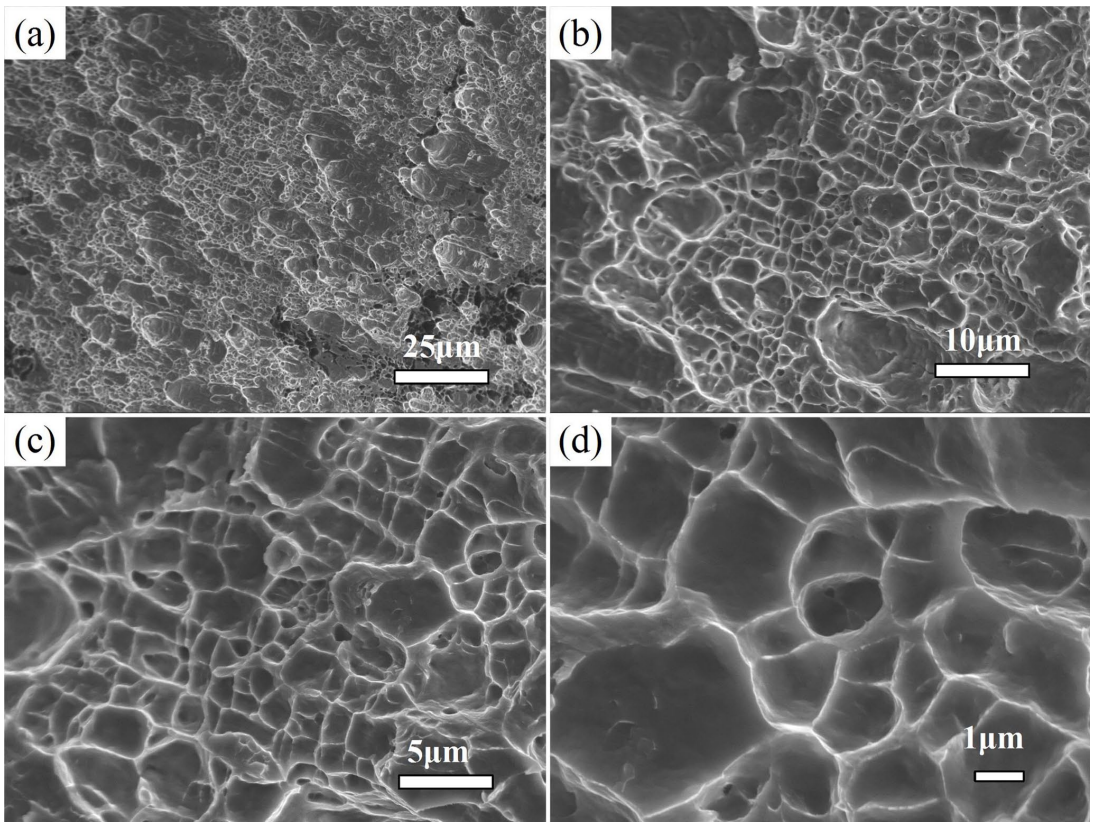

Fig. 8. Tensile fracture morphology of Cu-2.7Ti-2.5Ni-0.8V alloy after aging at 450°C for 240 min

REFERENCES

[1] S. Nevin Balo, M. Eskil, Appl. Phys. A **127**, 633 (2021).

[2] T. Kunimine, Y. Tomaru, M. Watanabe, R. Monzen, Mater. Trans. **62** (4), 479-483 (2021).

[3] K. Yildiz, Appl. Phys. A **126**, 422 (2020).

[4] B.M. Luo, D.X. Li, C. Zhao, Z. Wang, Z.Q. Luo, W.W. Zhang, Mater. Sci. Eng. A **746**, 154-161 (2019).

[5] Y.X. Liu, L. Wang, K. Jiang , S.T. Yang, J. Alloy Compd. **775**, 818-825 (2019).

[6] A.H. Huang, Y.F. Wang, M.S. Wang, L.Y. Song, Y.S. Li, L. Gao, C.X. Huang, Y.T. Zhu, Mater. Sci. Eng. A **746**, 211-216 (2019).

[7] L.K. Gong, H.C. Peng, X.Y. Wan, H.M. Chen, W.B. Xie, H. Wang, B. Yang, Mater. Sci. Technol. **35**, 1642-1650 (2019).

[8] A.I. Morozova, A.N. Belyakov, R.O. Kaibyshev, Phys. Met. Metallogr. **122**, 60-66 (2021).

[9] Y.J. Zhou, K.X. Song, J.D. Xing, Y.M. Zhang, J. Alloy Compd. **658**, 920-930 (2016).

[10] Y.J. Zhou, K.X. Song, J.D. Xing, Z. Li, X.H. Guo, Acta Metall. Sin. **29**, 399-408 (2016).

[11] Y.J. Zhou, K.X. Song, X.J. Mi, Y. Liu, S.D. Yang, Z. Li, Rare Metal Mat. Eng. **47** (4), 1096-1099 (2018).

[12] M. Sobhani, A. Mirhabibi, H. Arabi, R.M.D. Brydson Mater. Sci. Eng. A **577**, 16-22 (2013).

[13] A.A. Eze, T. Jamiru, E.R. Sadiku, M.O. Durowoju, W.K. Kupolati, I.D. Ibrahim, B.A. Obadele, P.A. Olubambi, S. Dioufbf, J. Alloy Compd. **736**, 163-171 (2018).

[14] Y.F. Geng, Y.J. Ban, X. Li, Y. Zhang, Y.L. Jia, B.H. Tian, M. Zhou, Y. Liu, A.A. Volinsky, K.X. Song, S.L. Tang, Mater. Sci. Eng. A **821**, 141639 (2021).

[15] C. Watanabe, S. Takeshita, R. Monzen, Metall. Mater. Trans. A **46**, 2469-2475 (2015).

[16] L. Huang, Z.S. Cui, X.P. Meng, X.W. Zhang, X.Y. Zhang, X.P. Song, N. Tang, Z. Xiao, Q. Lei, Z. Li, Mater. Sci. Eng. A, **823**, 141581 (2021).

[17] B. Rouxel, C. Cayron, J. Bornand, P. Sanders, R.E. Logéa, Mater. Design **213**, 110340 (2022).

[18] X. Wang, Z. Xiao, W.T. Qiu, Z. Li, F. Liu, Mater. Sci. Eng. A **803**, 140510 (2021).

[19] H.Y. Yang, Y.Q. Bu, J.M. Wu, Y.T. Fang, J.B. Liu, H.T. Wang, W. Yang, Mater. Charact. **176**, 111099 (2021).

[20] R. Markandeya, S. Nagarjuna, D.V.V. Satyanarayana, D.S. Sarma, Mater. Sci. Eng. A, **428** (1-2), 233-243 (2006).

[21] X.H. Wang, C.Y. Chen, T.T. Guo, J.T. Zou, Y.H. Yang, J. Mater. Eng. Perform. **24**, 2738-2743 (2015).

[22] T.J. Konno, R. Nishio, S. Semboshi, T. Ohsuna, E. Okunishi, J. Mater. Sci. **43**, 3761-3768 (2008).

[23] S. Kim, M. Kang. J. Ind. Eng. Chem. **18** (3), 969-978 (2012).

[24] J. Liu, X.H. Wang, J. Chen, J.T. Liu, J. Alloy Compd. **797**, 370-379 (2019).

[25] J. Liu, X.H. Wang, T.T. Guo, J.T. Zou, X.H. Yang, Int. J. Min. Met. Mate. **22**, 1199-1204 (2015).

[26] A. Takeuchi, A. Inoue, Mater. Trans. **46** (12), 2817-2829 (2005).

[27] K.J. Yuan, Y. Wang, L.J. Zheng, H. Zhang, J. Alloy Compd. **877**, 160263 (2021).

[28] K. Fujioka, Y. Kaneno, T. Takasugi, Mater. Sci. Eng. A **588** (24), 239-249 (2013).
[29] Z.K. Guo, J.C. Jie, S.C. Liu, Y.B. Zhang, B.L. Qin, T.M. Wang, T.J. Li, Mater. Sci. Eng. A, **748**, 85-94 (2019).
[30] X. Zhang, Q.S. Liu, Intermetallics, **92** 108-112 (2018).
[31] X.S. Xu, H.S. Ding, H.T. Huang, H. Liang, R.R. Chen, J.J. Guo, H.Z. Fu, Intermetallics, **142**, 107455 (2022).
[32] Y.W. Pan, A.P. Dong, Y. Zhou, D.F. Du, D.H. Wang, G.L. Zhu, B.D. Sun, J. Mater. Sci. Technol. **107**, 290-300 (2022).
[33] W.J. Liu, J. Li, X. Chen, M.H. Ji, X.P. Xiao, H. Wang, B. Yang, J. Mater. Res. Technol. **14**, 121-136 (2021).
[34] R. Badji, M. Bouabdallah, B. Bacroix, C. Kahloun, K. Bettahar, N. Kherroub, Mater. Sci. Eng. A **496 (1-2)**, 447-454 (2008).
[35] J.H. Su, P. Liu, H.J. Li, F.Z. Ren, Q.M. Dong, Mater. Lett. **61** (27), 4963-4966 (2007).
[36] Y. Pan, S.Q. Xiao, X. Lu, C. Zhou, Y. Li, Z.W. Liu, B.W. Liu, W. Xu, C.C. Jia, X.H. Qu, J. Alloy Compd. **782**, 1015-1023 (2019).
[37] J. Yi, Y.L. Jia, Y.Y. Zhao, Z. Xiao, K.J. He, Q. Wang, M.P. Wang, Z. Li, Acta Mater. **166**, 261-270 (2019).
[38] Q. Lei, Z. Li, C. Dai, J. Wang, X. Chen, J.M. Xie, W.W. Yang, D.L. Chen, Mater. Sci. Eng. A **572**, 65-74 (2013).
[39] C. Li, X.H. Wang, B. Li, J. Shi, Y.F. Liu, P. Xiao, J. Alloy Compd. **818**, 152915 (2020).
[40] R. Markandeya, S. Nagarjuna, D.S. Sarma, Mater. Charact. **57** (4-5), 348-357 (2006).
[41] R. Markandeya, S. Nagarjuna, D.S. Sarma, Mater. Charact. **54** (4-5), 360-369 (2005).